ChemComm

COMMUNICATION

View Article Online
View Journal | View Issue

Cite this: *Chem. Commun.*, 2022, **58**, 10687

Received 6th July 2022,
Accepted 23rd August 2022

DOI: 10.1039/d2cc03766a

rsc.li/chemcomm

Polyelectrolyte/surfactant films: from 2D to 3D structural control†

Javier Carrascosa-Tejedor, [ab] Andreas Santamaria, [ac] Andrea Tummino, [a] Imre Varga, [d] Marina Efstratiou, [b] M. Jayne Lawrence, [b] Armando Maestro *[ef] and Richard A. Campbell *[b]

Reversible control of the 3D structure of polyelectrolyte/surfactant films at the air/water interface is showcased. A recently discovered mechanism is exploited to form highly efficient, stable and biocompatible films by spreading aggregates composed of poly-L-lysine and sodium dodecyl sulfate on the surface of water. Reversible control of: (1) the surface monolayer coverage, (2) the switching on or off discrete extended structures, and (3) the extended structure coverage is demonstrated for the first time. The intricacy by which the film structures can be controlled is unprecedented and opens exciting potential to optimize film properties by chemical design for novel biomedical transfer applications.

The design of polymer-based nanofilms with controllable architecture attracts strong attention due to applications in areas such as biosensing,[1] tissue engineering[2] and drug delivery.[3] Preparation approaches include Langmuir Blodgett (LB) and Langmuir Schaeffer (LS) deposition onto solids from monolayers at the air/water interface,[4] the formation of layer-by-layer (LbL) films on solids,[5] and the formation of multilayer structures at both fluid and solid interfaces.[6] LB and LS deposition methods benefit from use of a Langmuir trough as the density, morphology and in-plane structures of films can be tuned prior to transfer.[7] While a transition from 2D to 3D structures has been reported in surfactant mixtures,[8] such an observation has not been made on polymer-based nanofilms to the knowledge of the authors. The development of new film formation methods is therefore of utmost importance.

A new approach to form polyelectrolyte/surfactant (P/S) films at the air/water interface was established a few years ago.[9] The approach involves dropping fresh aqueous dispersions of P/S aggregates onto the surface of water, which dissociate and spread material at the surface that remains kinetically trapped in a film due to the entropy associated with counterion release. The aggregates are pre-formed in P/S solutions at a molar ratio where complexes associate due to lack of colloidal stability,[10] initially with a size on the order of 100 nm.[9] Advantages of the approach include use of water as the spreading solvent and fast creation of films with a high amount of material compared with adsorbed layers, which offer both environmental and economic advantages in potential applications. Recent work showed that poly(sodium styrene sulfonate)/dodecyltrimethylammonium bromide (NaPSS/DTAB) aggregates can nucleate extended structures of different morphologies upon successive spreading or compression of the surface area, A.[11] The charge/structure of the aggregates determine if extended structures form, hence an interfacial mechanism where aggregates nucleate self-assembly of extended structures was inferred, conceptually analogous to the function of lung surfactant protein B during respiration.[12] Even so, a study limitation was that the extended structures were inferred from a surface excess, Γ, of surfactant exceeding its monolayer coverage, as a direct structural characterization was precluded due to their transient nature.

The aim of this work is to control 2D *versus* 3D structures in P/S spread films of relevance to biomedical transfer applications. The investigated mixture is poly-(L-lysine) (PLL) and sodium dodecyl sulfate (SDS). Both are biocompatible with PLL used in many biomedical applications such as complexing agents with DNA/siRNA for gene delivery,[13] and in cancer therapy,[14] while SDS is used in oral pharmaceutical formulations up to 1 wt%.[15] Also, they are used in film transfer applications such as PLL in a dual-responsive nanofluidic device,[16] to promote cellular adhesion,[17] and for skin regeneration,[18] and SDS in self-healing hydrogels.[19] An

[a] *Institut Laue-Langevin, 71 Avenue des Martyrs, CS20156, 38042 Grenoble, France*
[b] *Division of Pharmacy and Optometry, Faculty of Biology, Medicine and Health, University of Manchester, Oxford Road, Manchester M13 9PT, UK. E-mail: richard.campbell@manchester.ac.uk*
[c] *Departamento de Química Física, Facultad de Ciencias, Universidad Complutense de Madrid, Ciudad Universitaria s/n, 28040 Madrid, Spain*
[d] *Institute of Chemistry, Eötvös Loránd University, 112, Budapest H-1518, Hungary*
[e] *Centro de Física de Materiales (CSIC, UPV/EHU) - Materials Physics Center MPC, Paseo Manuel de Lardizabal 5, E-20018 San Sebastián, Spain. E-mail: armando.maestro@ehu.eus*
[f] *Basque Foundation for Science, Plaza Euskadi 5, Bilbao, 48009, Spain*

† Electronic supplementary information (ESI) available: (1) Zeta potential measurements of PLL/SDS aggregates, (2) materials and methods, (3) low-Q_z compositional analysis: fitting, (4) ellipsometry data on PLL/SDS spread film dynamics, (5) BAM images, (6) full-Q_z structural analysis: fitting and parameters, and (7) mid-Q_z structural dynamics analysis: fitting. See DOI: https://doi.org/10.1039/d2cc03766a

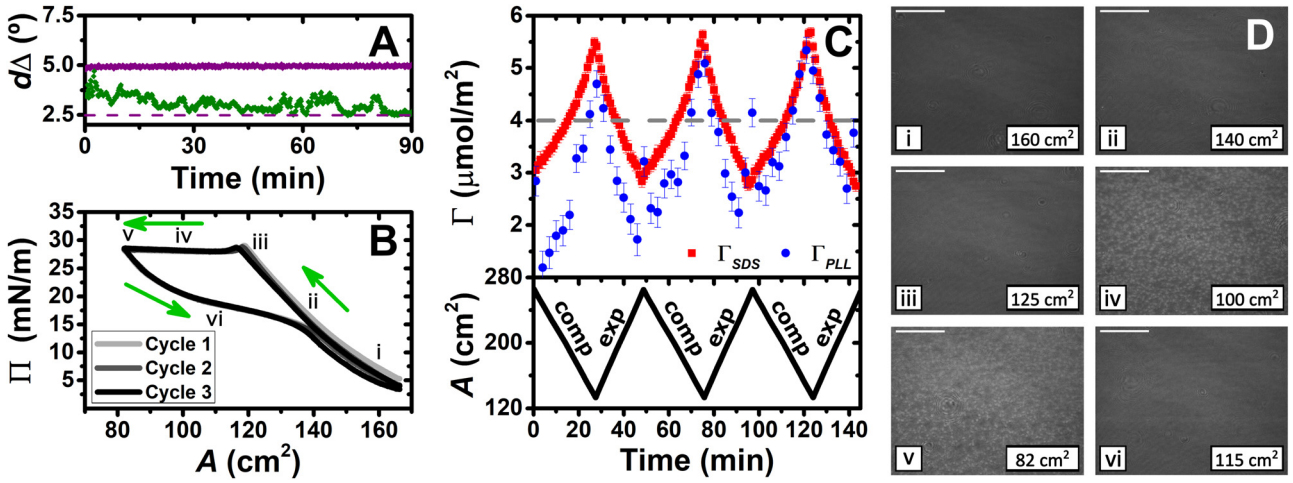

Fig. 1 (A) Variation of dΔ as a function of time for NaPSS/DTAB (green) and PLL/SDS (purple) films compressed by a factor of 2; purple dashed line indicates the dΔ value of a full monolayer of PLL/SDS or PSS/DTAB. (B) Variation of Π as a function of A; green arrows indicate the direction of area control and i–vi indicate different compression/expansion states. (C) Variation of the surface excess of PLL (blue circles) and SDS (red squares) from the low-Q_z analysis of NR during three cycles, and the area *versus* time (black lines); grey dashed line indicates Γ_{SDS} at the collapse. (D) BAM images of a PLL/SDS film corresponding to states i–v during compression and state vi during expansion as indicated in panel B; scale bars are 100 μm.

important pre-requisite of studying this system was that extended structures formed upon film compression are stable with time, allowing them to be characterized directly, and making them robust to potential applications. PLL was chosen over other polypeptides because in the bulk SDS can induce rigid in-plane interactions in a β-sheet conformation.[20] This pre-requisite was met, as ellipsometry data comparing compressed spread films of the NaPSS/DTAB and PLL/SDS systems show that only the latter type of film is stable (Fig. 1A).

Our methodology is to form a film by dispensing aqueous droplets containing PLL/SDS aggregates onto the water surface of a Langmuir trough and use barriers to control its surface area. The spreading solutions comprise 100 ppm PLL and 0.80 mM SDS, which self-assemble to form negatively charged aggregates as characterized by zeta potential (ESI,† Section S1), chosen simply because aggregates charged with excess surfactant are effective in forming extended structures for the NaPSS/DTAB system.[11] Several reflectometry techniques are applied to complement *in situ* measurements of the surface pressure, Π. Ellipsometry is used to measure the phase shift from the presence of the film, dΔ, which is related to the total amount of interfacial material per unit area.[21] Brewster angle microscopy (BAM) is used to image the lateral morphology on the μm-scale.[22] Three implementations of neutron reflectometry (NR) are applied to resolve the film composition and structure. First is the recently-developed low-Q_z analysis (0.01–0.03 Å^{-1}), where Q_z is the momentum transfer normal to the interface, to resolve the surface excesses of PLL and SDS during three compression/expansion cycles.[23] Second is the full-Q_z analysis (0.01–0.25 Å^{-1}) to resolve the interfacial structure at a high film compression state.[24] Third is a novel mid-Q_z analysis (0.02–0.12 Å^{-1}) to resolve the structural dynamics during one cycle. Full details about the materials and methods used are provided (ESI,† Section S2).

The dynamics of PLL/SDS spread films were first examined by combining measurements of Π with the low-Q_z analysis of NR, ellipsometry and BAM. First, the Π–A film response over three cycles is shown (Fig. 1B). Film compression initially results in a continuous increase in Π, attributed to enhanced molecular interactions with an increasing number of surfactant molecules per unit area in what we term the 'surface monolayer', *i.e.*, a layer of surfactant in contact with air (hydrophobic driving force) with hydrated polyelectrolyte bound to the headgroups (electrostatic driving force).[25] Upon further compression, beyond state iii, Π remains constant at ~28 mN m^{-1}, which is attributed to collapse of the surface monolayer, *i.e.* expulsion of material either to bound extended structures or the bulk. Expansion of the film is characterized by a large hysteresis in Π, the presence of a pseudo-plateau and a final value of Π close to the initial one, consistent with reincorporation of material back into the surface monolayer yet with a kinetic barrier.

The low-Q_z analysis of NR was applied to provide the surface excesses of PLL and SDS (Fig. 1C). An explanation of the fitting procedure is provided (ESI,† Section S3). In comparison with the value Γ_{SDS} = 4.0 ± 0.1 μmol m^{-2} at the collapse, upon further compression Γ_{SDS} continually rises to exceed this value. This observation demonstrates that the material expelled from the surface monolayer beyond the collapse remains bound in the form of extended structures rather than being lost to the bulk. From Γ_{SDS} = 5.5 ± 0.1 μmol m^{-2} at the maximum compression state measured, and with the assumption that Γ_{SDS} in the surface monolayer does not increase by further compression of the film after the collapse, it may be noted that 27 ± 1% of the SDS would be in the extended structures; we will return to this point later. Moreover, despite the large hysteresis in Π, there is no hysteresis in Γ, indicating that there are equivalent amounts of material in the film at corresponding

surface areas during compression or expansion, which suggests that the hysteresis is attributed to a kinetic barrier for the transfer of material from the extended structures to the surface monolayer. These results are supported qualitatively in values of dΔ recorded over successive cycles using ellipsometry (ESI,† Section S4). Lastly, the film composition over successive cycles is generally similar, hinting at their robustness to potential applications.

Next, we applied BAM to visualize the films (Fig. 1D). While prior to the collapse, images i, ii and iii are uniform with increasing brightness, images iv and v after exhibit discrete regions on the μm-scale that grow in number during compression, which we have reproduced in higher resolution combined with analysis of their coverage (ESI,† Section S5). The regions are attributed to discrete extended structures in contact with the surface monolayer and disappear in image vi upon expansion due to transfer of material back to the surface monolayer resulting in a homogeneous film once again.

A second implementation of NR exploiting the full Q_z-range allows us to resolve the extended structures of PLL/SDS films at maximum compression state v (Fig. 1B). Neutron reflectivity profiles in 4 isotopic contrasts with fits to a common interfacial model in stratified layers (Fig. 2A), and volume fraction (V_f) profiles (Fig. 2B) are shown. An explanation of the fitting procedure and a table of structural parameters is provided (ESI,† Section S6). A Kiessig fringe observed in data in the two isotopic contrasts that have the greatest scattering contrast between the surfactant chains and solvent, *i.e.*, PLL with deuterated SDS in air contrast matched water (ACMW, 8.1% v/v D_2O in H_2O) and PLL with SDS in D_2O (purple arrow), reveal the presence of extended structures with surfactant present below the surface monolayer. The extended structure layer has a thickness of 21.8 ± 0.8 Å (almost twice that of the SDS monolayer), and a model also involving PLL in the layer did not improve the fit. We infer that the structures are either discrete patches of SDS bilayer wrapped by unresolved PLL or bound SDS hemimicelles. The amount of SDS present in the extended structure is 29 ± 1%, consistent with the 27 ± 1% calculated above on the assumption that the surface monolayer does not change in coverage beyond the collapse. Although extended structures in adsorbed P/S layers have been recently the focus of an experimental study,[26] here we have resolved for the first time the extended structures of a P/S film formed by the aggregate spreading approach.

Lastly, we performed a third implementation of NR involving a novel mid-Q_z analysis to follow the structural dynamics of PLL/SDS films during one cycle. A single contrast of PLL with SDS in D_2O was chosen for maximum sensitivity to the surfactant in the extended structure (strong difference in scattering between the chains and solvent) compared with in the surface monolayer (weak difference in scattering between the chains and air). The scope is to resolve the change in thickness or coverage of the extended structures with respect to film compression. Data until the collapse (states i, ii and iii in Fig. 1B), combined with simulations of the reflectivity profiles based on the coverage of the surface monolayer from Fig. 1C, show that changing monolayer coverage indeed has a small effect on the data (Fig. 3A). However, data from the collapse (states iii, iv and v), combined with fits of the volume fraction at a constant extended structure thickness of 21.8 Å reveal the higher sensitivity of the measurements to the coverage of the extended structure (Fig. 3B). By comparison, fits of the data after the collapse to a model where the thickness of the extended structure changes at a constant volume fraction exhibited significantly worse agreement, as revealed by an increase of up to 30% in the global χ^2 parameter (ESI,† Section S7). It can be concluded that after collapse of the surface monolayer, the coverage of discrete patches of the wrapped bilayer or hemimicelles can now be controlled.

The coverage of extended structures, in comparison with the variation of Π, as a function of time is displayed (Fig. 3C).

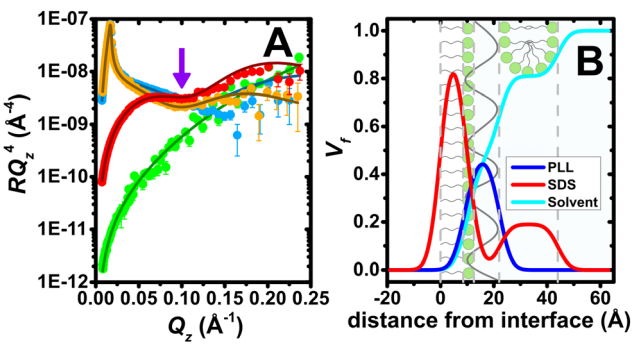

Fig. 2 (A) Neutron reflectivity profiles of a PLL/SDS spread film with deuterated SDS in D_2O (blue), SDS in D_2O (orange), deuterated SDS in ACMW (red), and SDS in ACMW (green); continuous lines show the model fits; purple arrow at Q_z = 0.1 Å^{-1} indicates a Kiessig fringe symptomatic of the extended structure. (B) Corresponding volume fraction profiles of PLL (blue), SDS (red) and solvent (cyan).

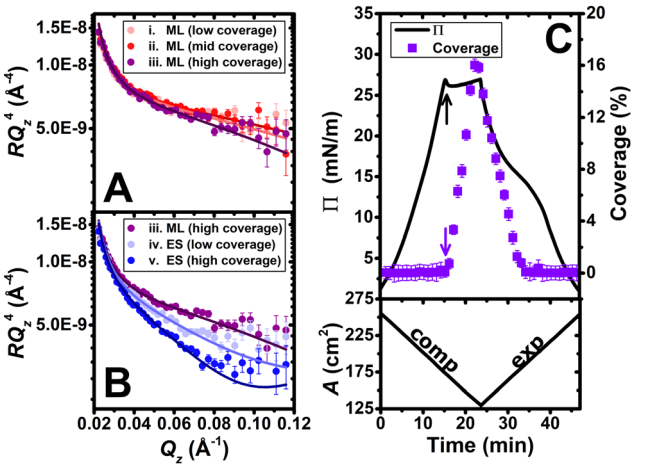

Fig. 3 Neutron reflectivity profiles of a PLL/SDS spread film in D_2O at different compression states: (A) monolayer (ML) region and (B) extended structure (ES) region; states i–v are defined in Fig. 1B; solid lines show the simulated ML models and fitted ES models. (C) Variation of Π (black line) and fitted extended structure coverage (violet squares) with respect to the time; black and violet arrows indicate film collapse and the onset of extended structures, respectively; variation of area *versus* time is also shown.

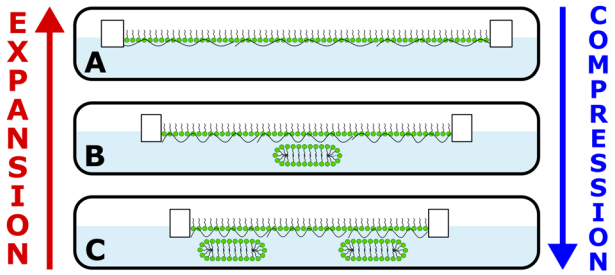

Fig. 4 Schematic illustration of (A) control of the coverage of the surface monolayer, (B) switching on or off 3D extended structures, and (C) control of the coverage of 3D extended structures.

The extended structures start to form (violet arrow) at the collapse (black arrow). The coverage increases with film compression beyond the collapse and decreases back down to 0% during the Π pseudo-plateau upon expansion, indicating that the surfactant in the extended structures has been fully resupplied to the monolayer. While the increase in coverage of extended structures takes ~7 min, the reduction takes ~10 min, consistent with the kinetic barrier to resupply of material to the surface monolayer. Although NR has been used previously to resolve changes in film composition under surface area dynamic,[9,11] this is the first time to the knowledge of the authors that it has been used to resolve changes in the extended structures of a dynamic air/water interface, and critically it highlights the unprecedented control gained over 2D *versus* 3D structures in P/S films, schematically illustrated (Fig. 4).

The PLL/SDS spread films studied in the present work are stable and reversible in their dynamics, which make them robust and amenable to transfer applications.[27] The combination of the new film spreading approach with established deposition techniques may offer economic and environmental advantages as the amount of materials used and waste generated are low compared to other methods.[28] As a result, 3D structures could be designed with controllable architecture and deposited onto solids for biomedical applications such as wound dressings, antimicrobial coatings or drug delivery applications.[29]

Coupling of reflectometry techniques to a Langmuir trough has allowed us to elucidate the compositional and structural dynamics and directly characterize the extended structures in P/S spread films for the first time. This approach must now be urgently applied to other systems to understand in greater depth the physicochemical film properties, such as by tuning specific amino acid interactions with reference to different polypeptide conformations adopted in the bulk (*e.g.* α-helices by polyarginine/SDS *versus* β-sheets by PLL/SDS).[20]

The mid-Q_z structural dynamic application of NR showcased in this study opens the possibility to understand a wide variety of synthetic and biological systems that adopt 3D morphologies. Further applications of the method include, for example, particle–laden interfaces that present buckling or jamming phenomena,[30] and lung surfactant models where the transfer of lipid between the surface monolayer and extended structures during respiration is vital for the stabilization of alveoli.[12]

We thank the Institut Laue-Langevin for beam time on FIGARO (DOIs: https://doi.org/10.5291/ILL-DATA.9-12-614 and https://doi.org/10.5291/ILL-DATA.9-12-631), Simon Wood for technical assistance and the Partnership for Soft Condensed Matter (PSCM) for lab support. IV acknowledges the financial support from the Hungarian National Research, Development and Innovation Office (NKFIH K116629). AM acknowledges the financial support from MICINN under grant PID2021-129054NA-I00 and the IKUR Strategy of the Basque Government.

Conflicts of interest

There are no conflicts of interest to declare.

References

1 W. Guan, W. Zhou, J. Lu and C. Lu, *Chem. Soc. Rev.*, 2015, **44**, 6981.
2 P. T. Hammond, *Mater. Today*, 2012, **15**, 196.
3 A. N. Zelikin, *ACS Nano*, 2010, **4**, 2494.
4 O. N. Oliveira, L. Caseli and K. Ariga, *Chem. Rev.*, 2022, **122**, 6459.
5 J. J. Richardson, J. Cui, M. Björnmalm, J. A. Braunger, H. Ejima and F. Caruso, *Chem. Rev.*, 2016, **116**, 14828.
6 R. A. Campbell, M. Yanez Arteta, A. Angus-Smyth, T. Nylander and I. Varga, *J. Phys. Chem. B*, 2012, **116**, 7981.
7 K. Ariga, *Langmuir*, 2020, **36**, 7158.
8 C. Rubia-Payá, E. Jimenez-Millán, J. J. Giner-Casares, G. Brezesinski, M. T. Martín-Romero and L. Camacho, *Langmuir*, 2013, **29**, 4796.
9 R. A. Campbell, A. Tummino, B. A. Noskov and I. Varga, *Soft Matter*, 2016, **12**, 5304.
10 R. Mészáros, L. Thompson, M. Bos, I. Varga and T. Gilányi, *Langmuir*, 2003, **19**, 609.
11 A. Tummino, J. Toscano, F. Sebastiani, B. A. Noskov, I. Varga and R. A. Campbell, *Langmuir*, 2018, **34**, 2312.
12 J. C. Castillo-Sánchez, A. Cruz and J. Pérez-Gil, *Arch. Biochem. Biophys.*, 2021, **703**, 108850.
13 B. Shi, M. Zheng, W. Tao, R. Chung, D. Jin, D. Ghaffari and O. C. Farokhzad, *Biomacromolecules*, 2017, **18**, 2231.
14 N. Li, L. Zhao, L. Qi, Z. Li and Y. Luan, *Prog. Polym. Sci.*, 2016, **58**, 1.
15 P. Y. Lin, E. Y. Chuang, Y. H. Chiu, H. L. Chen, K. J. Lin, J. H. Juang, C. H. Chiang, F. L. Mi and H. W. Sung, *J. Controlled Release*, 2017, **259**, 168.
16 J. Li, P. An, C. Qin, C. L. Sun, M. Sun, Z. Ji, C. Wang, G. Du, J. Liu and Y. Xie, *ACS Omega*, 2020, **5**, 4501.
17 P. P. Pokharna, M. K. Ghantasala and E. A. Rozhkova, *Mater. Today Commun.*, 2021, **27**, 102348.
18 J. Lam, E. C. Clark, E. L. S. Fong, E. J. Lee, S. Lu, Y. Tabata and A. G. Mikos, *Biomaterials*, 2016, **83**, 332.
19 D. C. Tuncaboylu, M. Sari, W. Oppermann and O. Okay, *Macromolecules*, 2011, **44**, 4997.
20 P. Novotná and M. Urbanová, *Anal. Biochem.*, 2012, **427**, 211.
21 J. A. De Feijter, J. Benjamins and F. A. Veer, *Biopolymers*, 1978, **17**, 1759.
22 W. Daear, M. Mahadeo and E. J. Prenner, *Biochim. Biophys. Acta, Biomembr.*, 2017, **1859**, 1749.
23 R. A. Campbell, *Curr. Opin. Colloid Interface Sci.*, 2018, **37**, 49.
24 M. W. A. Skoda, *Curr. Opin. Colloid Interface Sci.*, 2019, **42**, 41.
25 M. Uhlig, O. Löhmann, S. Vargas Ruiz, I. Varga, R. von Klitzing and R. A. Campbell, *Chem. Commun.*, 2020, **56**, 952.
26 L. Braun, M. Uhlig, O. Löhmann, R. A. Campbell, E. Schneck and R. von Klitzing, *ACS Appl. Mater. Interfaces*, 2022, **14**, 27347.
27 Y.-L. Lee, A. Dudek, T. N. Ke, F. W. Hsiao and C. H. Chang, *Macromolecules*, 2008, **41**, 5845.
28 J. Lipton, G. M. Weng, J. A. Röhr, H. Wang and A. D. Taylor, *Matter*, 2020, **2**, 1148.
29 M. A. C. Stuart, W. T. S. Huck, J. Genzer, M. Müller, C. Ober, M. Stamm, G. B. Sukhorukov, I. Szleifer, V. V. Tsukruk, M. Urban, F. Winnik, S. Zauscher, I. Luzinov and S. Minko, *Nat. Mater.*, 2010, **9**, 101.
30 B. D. Leahy, L. Pocivavsek, M. Meron, K. L. Lam, D. Salas, P. J. Viccaro, K. Y. C. Lee and B. Lin, *Phys. Rev. Lett.*, 2010, **105**, 058301.

